ARTICLE TYPE

Cite this: DOI: 00.0000/xxxxxxxxxx

Accumulation and ordering of P3HT oligomers at the liquid-vapor interface with implications for thin-film morphology†

Jakub K. Sowa,[a] Thomas C. Allen,[a] and Peter J. Rossky*[a]

Received Date
Accepted Date

DOI: 00.0000/xxxxxxxxxx

The morphology of semiconducting polymer thin films is known to have a profound effect on their opto-electronic properties. Although considerable efforts have been made to control and understand the processes which influence the structures of these systems, it remains largely unclear what physical factors determine the arrangement of polymer chains in spin-cast films. Here, we investigate the role that the liquid-vapor interfaces in chlorobenzene solutions of poly(3-hexylthiophene) [P3HT] play in the conformational geometries adopted by the polymers. Using all-atom molecular dynamics (MD), and supported by toy-model simulations, we demonstrate that, with increasing concentration, P3HT oligomers in solution exhibit a strong propensity for the liquid-vapor interface. Due to the differential solubility of the backbone and side chains of the oligomers, in the vicinity of this interface, hexyl chains and the thiophene rings, have a clear orientational preference with respect to the liquid surface. At high concentrations, we additionally establish a substantial degree of inter-oligomer alignment and thiophene ring stacking near the interface. Our results broadly concur with the limited existing experimental evidence and we suggest that the interfacial structure can act as a template for film structure. We argue that the differences in solvent affinity of the side chain and backbone moieties are the driving force for the anisotropic orientations of the polymers near the interface. This finer grained description contrasts with the usual monolithic characterization of polymer units. Since this phenomenon can be controlled by concurrent chemical design and the choice of solvents, this work establishes a fabrication principle which may be useful to develop more highly functional polymer films.

Introduction

Semiconducting polymers have found applications in a wide range of organic electronic devices including field effect transistors,[1,2] light-emitting diodes,[3–5] and perhaps most notably heterojunction solar cells.[6–8] P3HT has become a frequently studied model polymer in the context of solar cells primarily due to its favorable optoelectronic properties and relative ease of synthesis.[9] Of particular technological importance are the characteristics of P3HT thin ($\sim$ 300 nm) films typically produced using spin-coating, dip-coating, or drop-casting methods.[9] It is well established that a number of factors can significantly affect their morphology, and therefore also their optical and electronic properties. These include the molecular weight and regioregularity of the polymer,[10–12] the choice of solvent,[13,14] as well as the technique and conditions of the film deposition.[2,15] It has long been known, for instance, that electronic mobility in the P3HT films can vary over orders of magnitude depending on the used solvent,[13] underscoring the importance of phenomena occurring during the drying of the film. A higher degree of molecular order has generally been associated with higher carrier mobilities.[16,17] It is also believed that the level of ordering increases as the polymer chains adopt more equilibrated structures with a large degree of ring stacking and side chain interdigitation.[18] On that basis, slowly-evaporating

[a] Department of Chemistry, Rice University, Houston, TX 77005, USA.
* To whom correspondence should be addressed. E-mail: peter.rossky@rice.edu
† Electronic Supplementary Information (ESI) available. See DOI: 00.0000/00000000.

solvents,[14] slow spin casting rates,[19] and post-deposition film annealing[2,20] have all been used to fabricate polymer films with more desirable properties. Nonetheless, film depositions almost certainly produce non-equilibrium structures. However, due to the difficulty of simultaneously resolving all the relevant length and time scales, a mechanistic picture of this process, as well as the resulting mesoscale morphologies, is still missing. Consequently, optimization of the thin film fabrication practices remains necessarily empirical. Our inability to systematically control structure of such polymer films constitutes one of the main obstacles to practical technological applications of not just P3HT but semiconducting polymers more generally. This is true also for bulk heterojunction (most notably P3HT:PCBM) solar cells where the morphology of the blend film can have very large impact, for instance, on the undesirable carrier recombination processes.[21]

During drying, the polymer solution is exposed to two different interfaces, the solid-state substrate and the (highly non-polar) vapor interface, where at a separation of 100's of nm, uncorrelated physical evolution of the structure takes place as long as the polymer radius of gyration is small compared to this separation. Conformational ('edge-on' *vs.* 'face-on') ordering of polymer chains can be, in principle, established at either (or both) of these interfaces before propagating into the bulk. The influence of the substrate on the film morphology has been explored before,[11,22,23] using MD methods,[24,25] but focusing largely on the nature of the solid surface. In practice, however, one should expect that the behavior of polymer chains at either of the two interfaces is governed by the interplay between the polymer-solvent and polymer-substrate or vapor interactions. The phenomena occurring at the buried interface can also intricately depend on the atomistic structure of the top layers of the substrate which are often unknown and can vary from experiment to experiment. Furthermore, the phenomena taking place at the vapor interface of the (drying) solution will necessarily affect the morphology of the upper layers of the polymer film which can play a crucial role in the device performance.[26] Despite that, the phenomena occurring at the liquid-vapor interface of P3HT solutions, where solvent loss occurs, have not been extensively studied either experimentally or computationally. A handful of experimental studies have explored the air interface of P3HT thin films, yielding conflicting interpretations regarding the order in the upper layers of spin-coated films.[15,19,27–29]

Notably, Samuelsen *et al.* reported indirect evidence of accumulation of poly(octylthiophene) polymers near the air interface of their chloroform and toluene solutions.[30] Such skin layers[31] have also been observed in generic 'bead' models of polymer solutions[32,33] but their role in determining the morphology of P3HT films has thus far not been investigated.

In this work, we specifically investigate the behavior of P3HT in the vicinity of the liquid-vapor interface and the role it may play in the order and conformational alignment of P3HT chains. We make use of MD simulations and study a series of chlorobenzene solutions of P3HT in a slab geometry which provides two liquid-vapor interfaces, a useful means of establishing reproducibility of results. Given the existing evidence for polymer accumulation near the interface[30], we first focus on the case of an infinitely-dilute solution and investigate the orientational preferences of one oligomer when found near the liquid-vapor surface, as well as consider its propensity for residing in that vicinity. Although drying of a deposited film takes place on time scales far exceeding those accessible with MD simulations, as a spin-cast film dries, it necessarily passes through higher concentrations. We will therefore study the distribution and alignment of P3HT in increasingly concentrated solutions (which will serve as proxies for understanding the drying process) under the assumption that the structural rearrangements in the solution occur on much faster timescales than its drying. As we will demonstrate, this assumption is consistent with results of our simulations.

Results and Discussion

Infinite dilution

As discussed, we begin by establishing the behavior of a single 16-mer P3HT chain in a chlorobenzene slab at infinite dilution. The details of the simulations are outlined in the Methods section. We first investigate an oligomer's relative propensity for residing at the liquid-vapor interface in the form of a potential of the mean force (PMF) profile as a function of the oligomer-slab centers of mass distance. Figure 1(A) depicts the PMF (relative free energy) curve obtained using umbrella sampling;[34,36] also shown is the corresponding chlorobenzene density profile (chlorobenzene density as a function of distance from the center of the slab). We observe a flat potential within the slab core until the center of mass of the oligomer is roughly within 1 nm of the interface (defined as the distance at which the mean solvent density is half the bulk solvent density). This is followed by a relatively smooth increase of the potential until the plateau value (corresponding to the de-solvation free energy) is reached. We can see that the width of the PMF profile greatly exceeds that of the liquid-vapor interface (as inferred from the density profile). As the oligomer is pulled out of the chlorobenzene solution, it loses its solvation shell very gradually. This process results in a non-uniform distribution of the solvent; first as a bulge, and later as a neck-

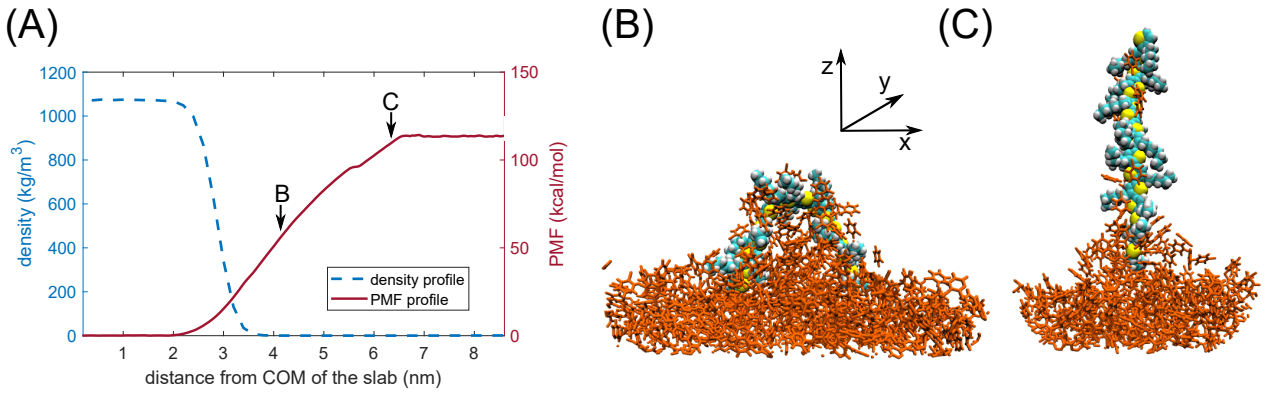

Fig. 1 (A) Potential of mean force profile for a single oligomer chain as a function of distance between its center of mass and that of the slab. Error on the PMF has been evaluated using bootstrapping trajectories based on umbrella histograms (200 bootstraps) [34] yielding errors below 0.4 kcal/mol throughout. Dashed line shows the chlorobenzene density profile from the final 4 ns of the pulling simulation (when the oligomer is entirely outside of the slab). (B, C) Snapshots from the pulling simulation showing (B) the solvent bulge, and (C) the solvent neck formed during the pulling-out of the oligomer from the slab. Visualisation were produced using VMD software. [35]

like structure; see Figures 1(B) and (C). Consequently, the bulk of the potential increase and desolvation takes place outside the nominal solution interface. One could in fact anticipate that the width of the PMF profile scales approximately linearly with the length of the oligomer. We also observe an inflection-like point around the separation of 5.5 nm; that distance corresponds to the transition between a roughly U-shaped and a linear geometry of the oligomer [which are shown in Figures 1 (B) and (C), respectively]. Furthermore, we note a lack of an energy minimum near the liquid-vapor interface. To additionally verify this, we performed three 30 ns simulations of a free oligomer (that is, in the absence of a biasing potential) in the chlorobenzene slab. As shown in Figure S2, at infinite dilution, the oligomer is indeed drawn to the bulk for maximum solvation – in contrast to what may occur at higher concentrations; [30] see below.

We proceed to examine the conformations adopted by the oligomer as a function of its position relative to that of the liquid-vapor interface. We will naturally focus on the orientations of the hexyl side chains and the thiophene rings with respect to the surface of the slab. To do so, we first define vectors describing the orientation of the hexyl chains and the thiophene rings, $\vec{r}_{hex}$ and $\vec{r}_{ring}$; see Figure 2(A) and the Methods section. We then examine the distribution of angles (labelled as ϕ and θ, respectively) between the $\vec{r}_{hex}$ and $\vec{r}_{ring}$ vectors and the z axis which is normal to the mean solvent interface, so that cosine equals one corresponds to a vapor pointing vector; see Figure 2(B).

As shown in Figures 2(C) and (D), when the center of mass of the oligomer is located more than 2 nm below the surface, we observe approximately uniform distributions of ϕ and θ angles. As the oligomer approaches the interface, its backbone aligns parallel to the surface [see Figure 2(B)] and clear trends in the conformations of the hexyl chains and thiophene rings emerge: The hexyl chains exhibit a strong preference to point towards the vapor phase [$\cos(\phi) > 0$], markedly so when the center of mass is found in the vicinity of the interface. This trend can be also seen in Figure 2(E) which depicts the mean and the median of the $\cos(\phi)$ distributions as a function of the center-of-mass position. Both of these quantities increase for increasing oligomer COM-surface distance and reach their maxima when the oligomer COM is located past the nominal solution interface – when the oligomer is held by the umbrella potential on a chlorobenzene bulge. Another trend is revealed in Figure 2(F) which shows the relative probabilities of the $\vec{r}_{hex}$ vectors being (approximately) parallel/antiparallel to the surface normal. We once again observe a clear preference for the 'upward' direction (towards the vapor phase). Somewhat surprisingly, however, the degree of alignment of hexyl vectors with the surface normal reaches its maximum at the COM position of around 0.7 nm below the surface. When the oligomer COM is held around 1 nm below the surface, an alignment of the hexyl chains parallel to the surface normal is necessary for the hexyl chains to extend into the vapor phase. On the other hand, in the close vicinity of (and past) the liquid interface, very small values of ϕ [$\cos(\phi) \sim 1$] are no longer imperative. The distribution at $\cos(\phi) \sim -1$ follows that at $\cos(\phi) \sim 1$ since, generally speaking, neighbouring side chains have a preference to point in opposite directions (due to the excluded volume driving the more stable polymer *trans* geometry). Secondly, as can be seen in Figure 2(D), the thiophene rings exhibit a propensity for aligning within the plane of the liquid surface [value of $\cos(\theta) \sim \pm 1$]. This is especially

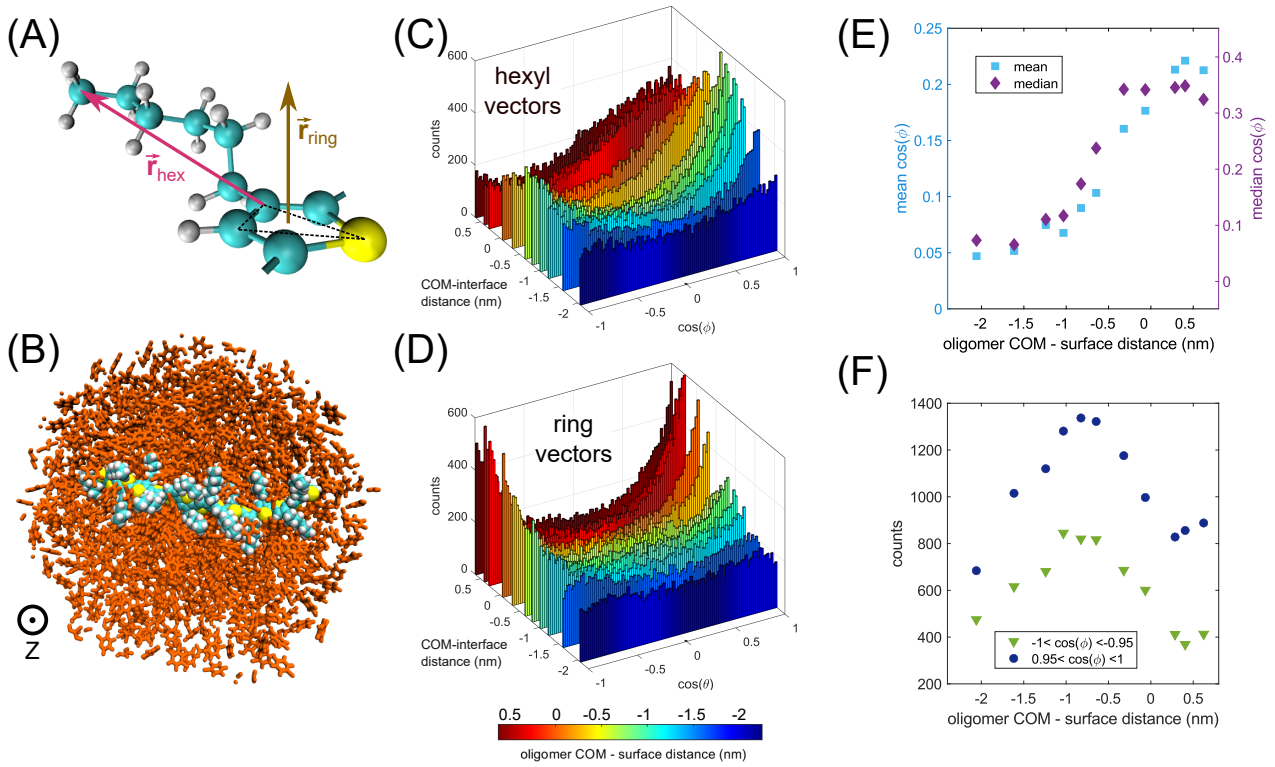

Fig. 2 (A) Definitions of the hexyl and thiophene ring vectors. (B) Top-down snapshot of the simulation for the oligomer center of mass position of -0.07 nm below the solvent-vapor interface. Distributions of angles of the hexyl (C) and thiophene ring (D) vectors with respect to the z direction (normal to the surface of the slab). (E) The mean and median of the $\cos(\phi)$ (hexyl vector angle) distributions as a function of the oligomer center-of-mass position with respect to the surface. (F) Counts of $\cos(\phi)$ values in the ranges of [-1, -0.95] and [0.95, 1].

pronounced in the close vicinity to the interface. We analyze this tendency quantitatively in Section S5 by fitting the $(\cos(\theta)+1)/2$ distributions to the beta probability function (chosen based on the empirical shape). As can be seen in Figure 2(D), and as we demonstrate in Figure S5, the propensity of the rings to align parallel to the liquid surface is strongest past the nominal interface, and correlates well with the 'upward' orientation of the hexyl chains, as quantified by the average value $\langle\cos(\phi)\rangle$.

The driving force behind these conformational preferences is evidently the differential solvation of the hexyl side chains and the thiophene backbone by chlorobenzene. We use the term *differential solubility* to capture the *relative* solvent affinity of the side chains compared to the polymer backbone, as it is that relative quantity that defines the orientational preference, rather than the solubilities, *per se*. The interactions between the less polar hexyl groups and the solvent are weaker than those between the backbone and the solvent (and those within the solvent itself), and are thus effectively unfavourable. The alignment of thiophene rings is a consequence of the (noticeably stronger) effect observed for the hexyl side chains. In order for most of the hexyl groups to point towards the vapor phase, while retaining the lower-energy *trans* configuration and the solvation of the thiophene rings, the rings in the oligomer align preferentially parallel to the surface of the slab.

We note here that observed orientation of the thiophene rings (parallel to the surface) is seemingly inconsistent with the experimental studies of surfaces of polymer films cast from chlorobenzene,[27,28,37] as discussed below.

Concentrated solutions

To understand the phenomena occurring during drying, and resolve the apparent inconsistencies between the infinite-dilution simulations and experimental studies of cast films, we next investigate the behaviour of oligomers at a finite concentration. We first consider a slab (once again with chlorobenzene as the solvent) with an effective nominal concentration of 100 mg/mL (or an approximately 14:1 chlorobenzene to 3HT ratio). For comparison, chlorobenzene solutions used for spin casting of P3HT thin films are typically prepared with initial concentrations between 2 and 10 mg/mL,[15,38–43] although concentrations as high as 60 mg/mL have been used.[44]

Initially, the oligomers are placed randomly within the

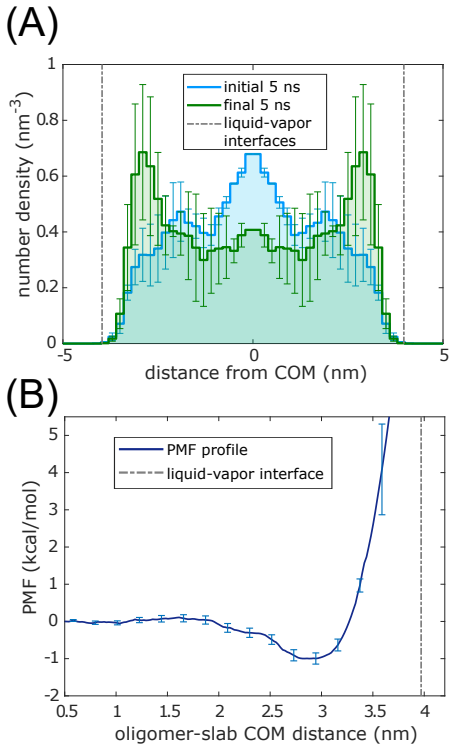

Fig. 3 (A) Symmetrised distributions of the positions of the sulfur atoms during the first (blue) and final (green) 5 ns of the (overall 40 ns) simulation of a nominally 100 mg/mL solution (symmetrisation with respect to center of the slab). The error bars indicate the lower/upper values obtained at respective distance away from the centre of the slab. (B) Potential of mean force for pulling of a single oligomer out of solution; *c.f.* Figure 1(A). The error was estimated using bootstrapping trajectories based on umbrella histograms with 200 bootstraps[34].

slab; Figure 3(A) shows the distribution of thiophene sulfur atoms during the first 5 ns of the simulation. After only $\sim$ 40 ns of relaxation, however, we observe an accumulation of the oligomers near the surfaces of the slab. The distribution of the sulfur atoms reaches its maximum around 1 nm below the interface, as does the distribution of the oligomer center-of-mass positions, see Figure S6. This is in contrast with the behavior in the infinite dilution limit. To further confirm this tendency, we calculate the PMF for pulling of the center-of-mass of one of the oligomers with respect to the remainder of the slab (see Section S3 for details), as shown in Figure 3(B). In contrast to the infinite-dilution case, there now exists a free energy minimum of around $k_{\mathrm{B}}T$ at 300 K. This minimum is located approximately 1 nm below the liquid-vapor interface, in agreement with the earlier unrestricted simulations. This confirms therefore that, at sufficiently high concentrations, P3HT oligomers have a tendency to accumulate near the liquid-vapor interface of their solution. Lastly, we note here the important observation that the changes in the distribution of oligomers within the slab occur much faster than the expected concentration variations due to drying, consistent with our earlier assumption.

What is the driving force behind this spontaneous accumulation? Since this behaviour is clearly concentration-induced, we can infer that its origin must lie in the polymer-polymer interactions. We investigate this hypothesis in Section S7 by constructing an effective model akin to the system considered in Figure 3. We describe the oligomers as particles whose motion is governed by the Langevin equation.[45] They are confined to a slab subject to a potential inferred from the infinite-dilution umbrella simulations and interact with each other via a repulsive soft-core Gaussian potential.[46–48] Physically, the origin of the latter interaction is entropic and arises from the excluded volume effect of polymers in a good solvent. Figure S8 shows the probability distributions of the locations of the particles within the slab and the corresponding potentials of mean force. At a concentration similar to the one used in Figure 3, we observe accumulation of particles near the two interfaces. The depth of the minima in the corresponding PMF profile agrees with that obtained from MD simulations.

Later stages of drying

We next investigate whether at later stages of drying, this accumulation can give rise to any degree of ordering among the oligomers near the interface. We consider slabs with a 2:1 and 1:1 ratios of chlorobenzene molecules to 3HT units. Following the creation of the slabs (which have a random distribution of oligomers), we perform a relaxation of these systems at 353 K. This higher temperature is used to accelerate the structural relaxation of the slab. We note however that such conditions are also sometimes used experimentally.[49]

We focus here on the more concentrated (1:1) slab; the intermediate results for the 2:1 slab are discussed in Section S9. Figure 4(A) shows the alignment of polymer chains at the top interface (within 2 nm of the solvent interface) following 650 ns of relaxation (the other interface is shown in Figure S9). We observe a certain level of oligomer adsorption and of oligomer-oligomer alignment.

We quantify the level of ordering of the hexyl chains by considering the order-parameter tensor Q given by

$$Q_{\alpha\beta} = \frac{1}{2N}\sum_i \left(3\, r_{hex,i}^{(\alpha)} r_{hex,i}^{(\beta)} - \delta_{\alpha\beta}\right) \qquad (1)$$

where the $r_{hex,i}$ vector components used are those of the normalized direction vectors, with components labelled by $\alpha,\beta = x,y,z$, and N is the number of considered vectors.[50]

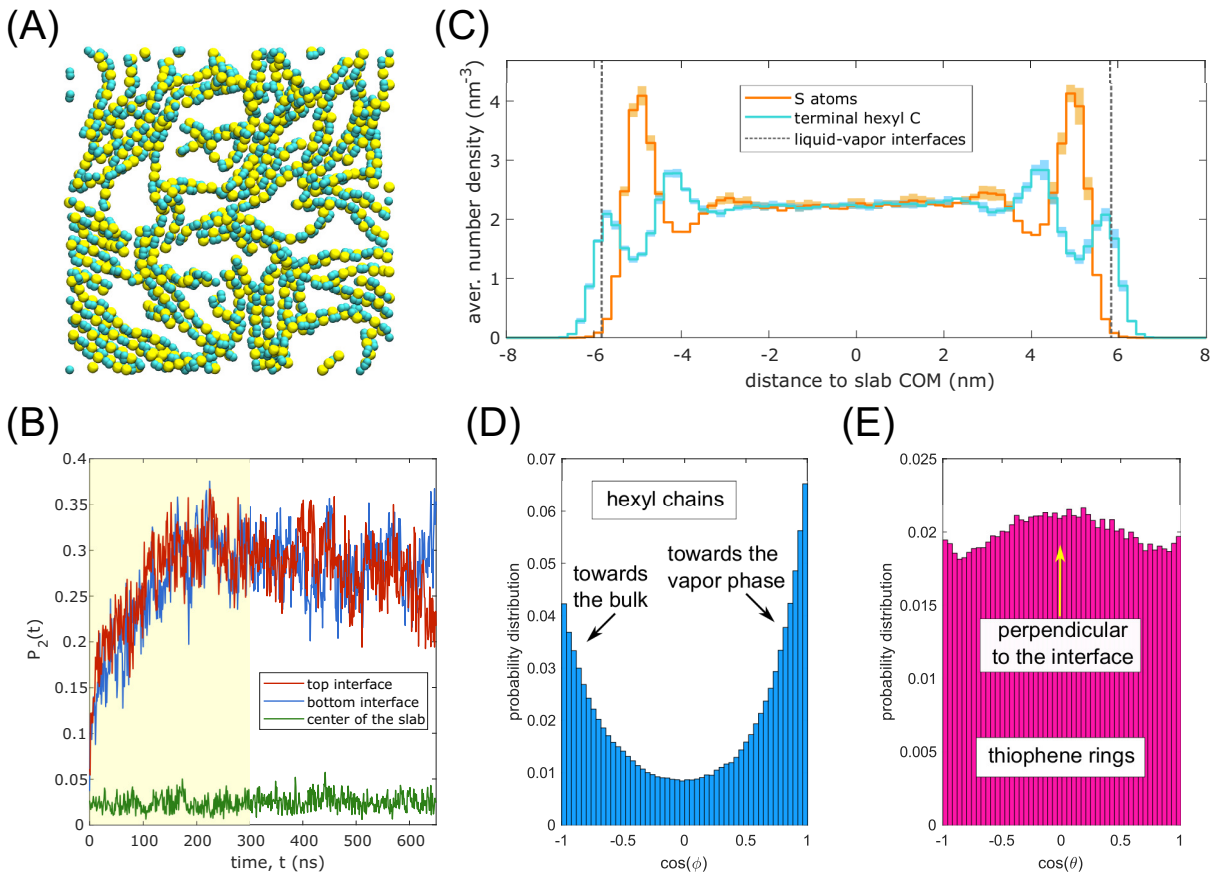

Fig. 4 Results from the simulations of the highly concentrated 1:1 slab. (A) View from the vapor phase of the geometry at the end of the production run (650 ns). Shown are the S, C2, and C3 atoms (see Figure 6) within 2 nm of the liquid-vapor (L/V) interface. (B) The hexyl order parameter $P_2(t)$ (Eq. 1) as a function of time for the two L/V interfaces and for a slice inside of the slab. (C) Distributions (unsymmetrized) of the sulfur atoms and the terminal hexyl carbon atoms over the course of the production run. The shading indicates standard deviation error obtained from 50 ns segments. (D, E) Distributions of the angles between (D) hexyl and (E) ring vectors and the vapor phase-pointing normal to the plane of the slab provided the relevant ring center is found within 1.5 nm of an L/V interface. For panels (C-E), the first 300 ns are discarded as relaxation [as indicated in panel (B)].

The largest eigenvalue of Q corresponds to the order parameter, $P_2(t)$. In Figure 4(B), we plot $P_2(t)$ as a function of the relaxation time and subdivided based on the position of the corresponding ring center, defining the interfacial regions as within 1.5 nm from either interface. The ordering of the hexyl vectors at the interfaces increases over the first 200 ns while the hexyl chains in the middle (remaining) part of the slab remain essentially isotropically oriented throughout the course of the simulation.

Figure 4(C) depicts the distributions of the sulfur and the terminal hexyl carbon atoms during the 350 ns following the 300 ns of relaxation. We again find that the P3HT oligomers are accumulated in the vicinity of the interfaces forming a layer-like structure just below the surface of the solution with the alkyl chains extending either towards the vapor phase or towards the bulk. Notably, we also observe formation of distinct secondary layers. Their presence is evidenced by the anti-correlated oscillations of the sulfur and terminal alkyl carbon distributions. It is important to note that this layering via alternation of rings and sidechains, with overlapping alkyl chains and an edge-on ring orientation, is completely consistent with the observed structure in crystalline microwires of P3HT.[18]

In Figures 4(D) and (E), we show the results of the orientational analysis described above for an isolated interfacial oligomer, but now in this concentrated system. The oligomers in the interfacial layer align now in an 'edge-on' fashion: Similarly to what was found in the infinite dilution limit, the hexyl chains exhibit an evident preference for pointing towards the vapor phase and to a lesser extent towards the bulk. However, when numerous at the interface, there exists a preference for the thiophene rings to align perpendicularly to the surface of the solution which gives rise to efficient packing.

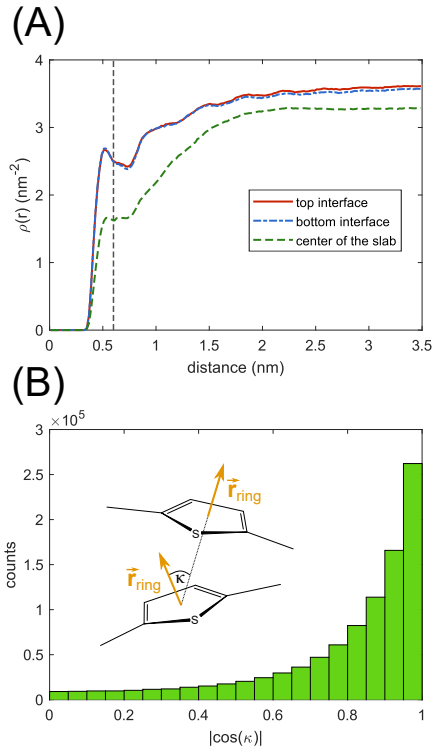

Fig. 5 (A) Radial distribution function for thiophene rings within 1.5 nm of the top/bottom interface and in a 1.5 nm region in the centre of the slab, calculated disregarding rings on the same chain. (B) Histogram of angles between neighbouring rings (see inset for definition) within 1.5 nm of the top interface. As in Figure 4, the first 300 ns is discarded as relaxation.

We next investigate the degree of thiophene ring stacking near the surfaces of the concentrated solution. We first consider the distances between the centers of thiophene rings by calculating the radial density function, $\rho(r)$ (see Section S10). The radial density functions (calculated excluding thiophene rings on the same oligomer chain) are plotted in Figure 5(A). The data reveals ring-ring stacking in radial density function peaks at $r \approx 0.5$ nm and multiples, which is the evident stacking distance. Evidence for several layers (due to the presence of a handful of noticeable maxima) can be observed. While the radial density functions appear qualitatively identical at the two interfaces, one also sees that $\rho(r)$ exhibits little structure in the bulk which implies a low degree of ring stacking and aggregation in the middle of the slab. This indicates that, during drying, thiophene stacking most likely occurs at the liquid-vapor interface before it does in the bulk. We can then consider the extent to which the stacked thiophene rings near the interfaces are parallel to each other. Using the radial distribution functions, we define two rings as "stacked" if the ring-ring distance falls below the cut off of $r_0 = 0.6$ nm – the vertical dashed line in Figure 5(A). In Figure 5(B), we plot the distribution of $|\cos(\kappa)|$ values where κ is the angle between the vectors normal to the two stacked thiophene rings. We observe that the rings exhibit a high degree of alignment, as anticipated.

The analysis of the less concentrated (2:1) slab reveals largely similar behaviour, see Section S9. However, due to the lower concentration of P3HT (in the bulk and consequently also in the vicinity of the interfaces), the thiophene rings exhibit little preference for stacking and preferentially align parallel to the liquid-vapor interfaces (similarly to the infinite-dilution case); see Figure S12. Experimentally, one should therefore expect a transition from a predominantly parallel to a perpendiuclar orientation of the thiophene rings during the later stages of drying as the polymers begin adopting stacked geometries.

The results presented here are consistent with those of Wei *et al.* who reported high electronic mobilities (implying a propensity for stacking) of the outer surface of P3HT films spin coated from chlorobenzene.[28,29] Additionally, in agreement with our results, Ho *et al.* observed a preference for edge-on alignment of thiophene rings near the air interface of P3HT films cast from chlorobenzene.[27] These authors have also reported a near isotropic distribution of alkyl C-C bonds near the interface. We note however that, due to the fluctuations and geometry of the alkyl chains, the angular distribution of the carbon-carbon bonds does not accurately reflect the overall orientation of the hexyl side chains. We have also performed analogous slab simulations of solutions of P3HT in chloroform, see Section S11. They reveal a similar tendency for accumulation of oligomers near the liquid-vapor interface. Our simulations of highly concentrated P3HT chloroform solutions predict that their upper-most layer similarly consists primarily of hexyl side chains in apparent agreement with the surface-sensitive studies of Hao *et al.*[19]

To demonstrate how the properties of the solvent can influence the effects discussed here, we performed a simulation of the slab with the 2:1 ratio of chlorobenzene to 3HT in which we fictitiously doubled the partial charges on the chlorobenzene molecules (thus increasing the solvent polarity). As discussed in Section S12, this results in a significantly stronger tendency for the oligomers to accumulate at the liquid-vapor interfaces, a higher degree of thiophene stacking, and a more pronounced orientational ordering (as compared to the slab of less polar solvent at the same concentration). This illustrates that increasing the polarity of the solvent can enhance the effects discussed here by enhancing the differential solvation between rings and sidechains.

Conclusions

In this work, we investigated the liquid-vapor interfaces of P3HT solutions in chlorobenzene. We have shown that due to oligomer-oligomer interactions, at higher concentrations, P3HT chains accumulate in the vicinity of the liquid-vapor interface. We stress that this process should be unavoidable since the concentration of the cast solution must increase as the drying of the film progresses. In this region, oligomers exhibit clear conformational preferences. We find that the hexyl side chains have the propensity to extend towards the vapor phase. The thiophene rings tend to align parallel to the interface at low density (presumably to allow for the more favourable alignment of the hexyl chains) and perpendicular to the interface at high concentrations leading to a more efficient ('edge-on') packing. Our results broadly agree with the limited existing experimental studies. We suggest that the structures established at the surfaces of P3HT solutions may serve as a template for those forming in the bulk film as solvent evaporates further. We also note that the air interfaces of P3HT:PCBM thin films (cast from chlorobenzene as well as chloroform solutions) are typically observed experimentally to be comprise almost exclusively P3HT chains.[51–53] Not only does this indicate a clear preference for P3HT (over PCBM) to accumulate near the interfaces of concentrated blend solutions, but it additionally suggests that the differential-solvation driven phenomena investigated here may also play an important role in the morphology of bulk heterojunction solar cell films.

This work suggests a new paradigm for the design of semiconducting polymers, as well as for the choice of solvent used in the thin film preparation, based on the *differential* solubility of the side chains and the polymer backbone. As we have demonstrated throughout this work, the proximity of the oligomers to the liquid-vapor interface results in a substantial degree of conformational alignment, driven by the differences, *within* each monomer, between the backbone-solvent and side chain-solvent interactions. It should, in principle, be possible to tune these differences by means of chemical design and rational choice of solvent or mixed solvents. In mixed solvents, one has the possibility, in essence, of continuous tuning of the solvent quality, although preferential (non-random) local solvation structure may add complexity to the response, and simulations which reliably sample statistical distributions are considerably more demanding than in a one-component solvent.[54] This could then be exploited to obtain an increased degree of conformational order and potentially more favorable optoelectronic properties of the entire thin film.

Finally, our hope is that this study will prompt detailed real-time investigations of drying P3HT and related polymer solutions. Surface-sensitive techniques such as X-ray reflectivity[55] and time-resolved sum frequency generation spectroscopy (especially when focusing on the orientations of the thiophene rings rather than alkyl bonds)[37,56,57] could provide important clues regarding the progression of interfacial accumulation and alignment of P3HT or similar polymer chains near the surfaces of their solutions.

Methods

The Molecular Dynamics simulations were performed using GROMACS 2020 software.[58] We use the leap frog algorithm and a 2 fs step size throughout. Unless stated otherwise, all simulations were performed in an NVT ensemble using velocity rescaling thermostat[59] (at $T = 300$ K, with $\tau_T = 0.1$ ps). We make use of the LINCS algorithm with constrains only on H-covalent bonds.[60] Remaining simulation details are given in the Supporting Information.

We make use of the all-atom OPLS force field[61] as the underlying model. The partial charges for the P3HT oligomer and the chlorobenzene molecules were taken from Tummala *et al.*[62] and Jorgensen *et al.*,[63] respectively. The force field parameters were obtained using the LigParGen tool.[64,65]

To validate the force field, we considered a P3HT 16-mer in gas phase and in a chlorobenzene solution and investigated the distribution of S-C-C-S dihedral angles which are an important (but non-trivial to parametrize[66]) characteristics of poly-thiophene polymers. As shown in Figure S1, the conventional OPLS force field yields the positions of the maxima (at dihedral angles of roughly $\pm 40^\circ$ and $\pm 145^\circ$) as well as the relative *cis*:*trans* population ratios that agree well with the literature.[67–69] We also considered the density of chlorobenzene in the slab (in the absence of P3HT) which reproduces the experimental density at atmospheric pressure within 2.5% of the experimental density of the bulk solvent.[70]

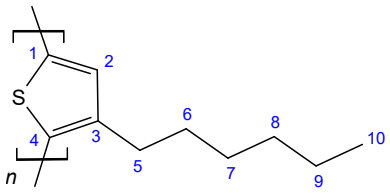

Fig. 6 The structure of a 3HT unit.

A number of vectors were used to quantify the conformational and inter-chain alignment. The hexyl vector is defined as $\vec{r}_{hex} = \vec{r}_{C10} - \vec{r}_{C3}$ and the ring vector is given by the cross product $\vec{r}_{ring} = (\vec{r}_{C2} - \vec{r}_S) \times (\vec{r}_{C3} - \vec{r}_S)$, see Figure 6. The center of the ring i is defined as the average $\vec{r}_i = (\vec{r}_S + \vec{r}_{C2} + \vec{r}_{C3})/3$.

Author Contributions

JKS, TCA, and PJR designed research. JKS and PJR performed research, analyzed data, and wrote the paper.

Conflicts of interest

There are no conflicts to declare.

Data Availability

Additional simulation data and topology files are available in the Supporting Information and from the open access repository `https://figshare.com/articles/dataset/Trajectory_and_topology_files_for_MD_simulations_of_P3HT/21817578`

Acknowledgements

This work was supported by the Center for Adapting Flaws into Features, an NSF Center for Chemical Innovation supported by grant CHE-2124983 and by the Big-Data Private-Cloud Research Cyberinfrastructure MRI award funded by the NSF under grant CNS-1338099 and by Rice University's Center for Research Computing (CRC). We also gratefully acknowledge High Performance Computing (HPC) resources and support provided to Rice University by Advanced Micro Devices (AMD).

Notes and references

1 F. Garnier, R. Hajlaoui, A. Yassar and P. Srivastava, *Science*, 1994, **265**, 1684–1686.

2 G. Wang, J. Swensen, D. Moses and A. J. Heeger, *J. Appl. Phys.*, 2003, **93**, 6137–6141.

3 P. K. Ho, J.-S. Kim, J. H. Burroughes, H. Becker, S. F. Li, T. M. Brown, F. Cacialli and R. H. Friend, *Nature*, 2000, **404**, 481–484.

4 I. D. Parker, *J. Appl. Phys.*, 1994, **75**, 1656–1666.

5 J. H. Burroughes, D. D. Bradley, A. Brown, R. Marks, K. Mackay, R. H. Friend, P. L. Burns and A. B. Holmes, *Nature*, 1990, **347**, 539–541.

6 G. Li, R. Zhu and Y. Yang, *Nat. Photon.*, 2012, **6**, 153–161.

7 F. Padinger, R. S. Rittberger and N. S. Sariciftci, *Adv. Funct. Mater.*, 2003, **13**, 85–88.

8 G. Yu, J. Gao, J. C. Hummelen, F. Wudl and A. J. Heeger, *Science*, 1995, **270**, 1789–1791.

9 S. e. Ludwigs, *P3HT Revisited-From Molecular Scale to Solar Cell Devices*, Springer, 2014, vol. 265.

10 H. Yang, T. Joo Shin, Z. Bao and C. Y. Ryu, *J. Polym. Sci. Part B: Polym. Phys.*, 2007, **45**, 1303–1312.

11 R. J. Kline, M. D. McGehee and M. F. Toney, *Nat. Mater.*, 2006, **5**, 222–228.

12 J.-M. Verilhac, G. LeBlevennec, D. Djurado, F. Rieutord, M. Chouiki, J.-P. Travers and A. Pron, *Synth. Met.*, 2006, **156**, 815–823.

13 Z. Bao, A. Dodabalapur and A. J. Lovinger, *Appl. Phys. Lett.*, 1996, **69**, 4108–4110.

14 J.-F. Chang, B. Sun, D. W. Breiby, M. M. Nielsen, T. I. Sölling, M. Giles, I. McCulloch and H. Sirringhaus, *Chem. Mater.*, 2004, **16**, 4772–4776.

15 D. M. DeLongchamp, B. M. Vogel, Y. Jung, M. C. Gurau, C. A. Richter, O. A. Kirillov, J. Obrzut, D. A. Fischer, S. Sambasivan, L. J. Richter *et al.*, *Chem. Mater.*, 2005, **17**, 5610–5612.

16 A. J. Sneyd, T. Fukui, D. Paleček, S. Prodhan, I. Wagner, Y. Zhang, J. Sung, S. M. Collins, T. J. Slater, Z. Andaji-Garmaroudi *et al.*, *Sci. Adv.*, 2021, **7**, eabh4232.

17 D. P. McMahon and A. Troisi, *Chem Phys Chem*, 2010, **11**, 2067–2074.

18 L. Zhai, S. I. Khondaker, J. Thomas, C. Shen and M. McInnis, *Nano Today*, 2014, **9**, 705–721.

19 X. Hao, T. Hosokai, N. Mitsuo, S. Kera, K. Okudaira, K. Mase and N. Ueno, *J. Phys. Chem. B*, 2007, **111**, 10365–10372.

20 S. Cho, K. Lee, J. Yuen, G. Wang, D. Moses, A. J. Heeger, M. Surin and R. Lazzaroni, *J. Appl. Phys.*, 2006, **100**, 114503.

21 S. Wilken, D. Scheunemann, S. Dahlström, M. Nyman, J. Parisi and R. Österbacka, *Adv. Electron. Mater.*, 2021, **7**, 2001056.

22 B. J. Boehm, H. T. Nguyen and D. M. Huang, *J. Phys. Condens. Matter*, 2019, **31**, 423001.

23 G. Scavia, L. Barba, G. Arrighetti, S. Milita and W. Porzio, *Eur. Polym. J.*, 2012, **48**, 1050–1061.

24 B. Meredig, A. Salleo and R. Gee, *ACS Nano*, 2009, **3**, 2881–2886.

25 S. Obata and Y. Shimoi, *Phys. Chem. Chem. Phys.*, 2013, **15**, 9265–9270.

26 K. Nakano and K. Tajima, *Adv. Mater.*, 2017, **29**, 1603269.

27 P.-H. Ho, L.-L. Chua, M. Dipankar, X. Gao, D. Qi, A.-S. Wee, J.-F. Chang and R. H. Friend, *Adv. Mater.*, 2007, **19**, 215–221.

28 Q. Wei, S. Miyanishi, K. Tajima and K. Hashimoto, *ACS Appl. Mater. Interfaces*, 2009, **1**, 2660–2666.

29 Q. Wei, K. Tajima and K. Hashimoto, *Appl. Phys. Lett.*, 2010, **96**, 110.

30 E. J. Samuelsen, D. W. Breiby, O. Konovalov, B. Struth and D.-M. Smilgies, *Synth. Met.*, 2001, **123**, 165–170.

31 P. G. De Gennes, *Eur. Phys. J. E Soft Matter*, 2002, **7**, 31–34.

32 M. Tsige and G. S. Grest, *Macromolecules*, 2004, **37**, 4333–4335.

33 A. Statt, M. P. Howard and A. Z. Panagiotopoulos, *J. Chem. Phys.*, 2017, **147**, 184901.

34 J. S. Hub, B. L. De Groot and D. Van Der Spoel, *J. Chem. Theory Comput.*, 2010, **6**, 3713–3720.

35 W. Humphrey, A. Dalke and K. Schulten, *J. Mol. Graph.*, 1996, **14**, 33–38.

36 G. M. Torrie and J. P. Valleau, *J. Comput. Phys.*, 1977, **23**, 187–199.

37 J. N. Myers, C. Zhang, C. Chen and Z. Chen, *J. Colloid Interface Sci.*, 2014, **423**, 60–66.

38 N. Seidler, G. M. Lazzerini, G. L. Destri, G. Marletta and F. Cacialli, *J. Mater. Chem. C*, 2013, **1**, 7748–7757.

39 P. Ehrenreich, S. T. Birkhold, E. Zimmermann, H. Hu, K.-D. Kim, J. Weickert, T. Pfadler and L. Schmidt-Mende, *Sci. Rep.*, 2016, **6**, 1–8.

40 E. Verploegen, R. Mondal, C. J. Bettinger, S. Sok, M. F. Toney and Z. Bao, *Adv. Funct. Mater.*, 2010, **20**, 3519–3529.

41 E. Verploegen, C. E. Miller, K. Schmidt, Z. Bao and M. F. Toney, *Chem. Mater.*, 2012, **24**, 3923–3931.

42 U. Bielecka, P. Lutsyk, K. Janus, J. Sworakowski and W. Bartkowiak, *Org. Electron.*, 2011, **12**, 1768–1776.

43 R. Wei, M. Gryszel, L. Migliaccio and E. D. Głowacki, *J. Mat. Chem. C*, 2020, **8**, 10897–10906.

44 T. Agostinelli, M. Campoy-Quiles, J. Blakesley, R. Speller, D. Bradley and J. Nelson, *Appl.Phys. Lett.*, 2008, **93**, 419.

45 R. Zwanzig, *Nonequilibrium statistical mechanics*, Oxford University Press, 2001.

46 P. Flory and W. Krigbaum, *J. Chem. Phys.*, 1950, **18**, 1086–1094.

47 C. N. Likos, *Phys. Rep.*, 2001, **348**, 267–439.

48 P. Bolhuis, A. Louis, J. Hansen and E. Meijer, *J. Chem. Phys.*, 2001, **114**, 4296–4311.

49 D. T. Duong, C. Wang, E. Antono, M. F. Toney and A. Salleo, *Org. Electron.*, 2013, **14**, 1330–1336.

50 M. P. Allen and D. J. Tildesley, *Computer simulation of liquids*, Oxford University Press, 2017.

51 A. F. Tillack, K. M. Noone, B. A. MacLeod, D. Nordlund, K. P. Nagle, J. A. Bradley, S. K. Hau, H.-L. Yip, A. K.-Y. Jen, G. T. Seidler and D. S. Ginger, *ACS Appl. Mater. Interfaces*, 2011, **3**, 726–732.

52 B. Xue, B. Vaughan, C.-H. Poh, K. B. Burke, L. Thomsen, A. Stapleton, X. Zhou, G. W. Bryant, W. Belcher and P. C. Dastoor, *J. Phys. Chem. C*, 2010, **114**, 15797–15805.

53 Z. Xu, L.-M. Chen, G. Yang, C.-H. Huang, J. Hou, Y. Wu, G. Li, C.-S. Hsu and Y. Yang, *Adv. Funct. Mater.*, 2009, **19**, 1227–1234.

54 N. F. van der Vegt and D. Nayar, *J. Phys. Chem. B*, 2017, **121**, 9986–9998.

55 E. Chason and T. Mayer, *Critical Reviews in Solid State and Material Sciences*, 1997, **22**, 1–67.

56 Z. Chen, Y. Shen and G. A. Somorjai, *Ann. Rev. Phys. Chem.*, 2002, **53**, 437–465.

57 M. J. Schultz, S. Baldelli, C. Schnitzer and D. Simonelli, *J. Phys. Chem. B*, 2002, **106**, 5313–5324.

58 H. J. Berendsen, D. van der Spoel and R. van Drunen, *Comput. Phys. Commun.*, 1995, **91**, 43–56.

59 G. Bussi, D. Donadio and M. Parrinello, *J. Chem. Phys.*, 2007, **126**, 014101.

60 B. Hess, H. Bekker, H. J. Berendsen and J. G. Fraaije, *J. Comput. Chemistry*, 1997, **18**, 1463–1472.

61 W. L. Jorgensen, D. S. Maxwell and J. Tirado-Rives, *J. Am. Chem. Soc.*, 1996, **118**, 11225–11236.

62 N. R. Tummala, C. Bruner, C. Risko, J.-L. Bredas and R. H. Dauskardt, *ACS Appl. Mater. Interfaces*, 2015, **7**, 9957–9964.

63 W. L. Jorgensen and P. Schyman, *J. Chem. Theory Comput.*, 2012, **8**, 3895–3901.

64 W. L. Jorgensen and J. Tirado-Rives, *Proc. Natl. Acad. Sci. U.S.A.*, 2005, **102**, 6665–6670.

65 L. S. Dodda, I. Cabeza de Vaca, J. Tirado-Rives and W. L. Jorgensen, *Nucleic Acids Res.*, 2017, **45**, W331–W336.

66 K. H. DuBay, M. L. Hall, T. F. Hughes, C. Wu, D. R. Reichman and R. A. Friesner, *J. Chem. Theory Comput.*, 2012, **8**, 4556–4569.

67 L. Simine and P. J. Rossky, *J. Phys. Chem. Lett.*, 2017, **8**, 1752–1756.

68 D. Khlaifia, C. P. Ewels, F. Massuyeau, M. Chemek, E. Faulques, J.-L. Duvail and K. Alimi, *RSC Adv.*, 2016, **6**, 56174–56182.

69 S. Y. Son, Y. Kim, J. Lee, G.-Y. Lee, W.-T. Park, Y.-Y. Noh, C. E. Park and T. Park, *J. Am. Chem. Soc.*, 2016, **138**, 8096–8103.

70 P. S. Nikam and S. J. Kharat, *Journal of Chemical & Engineering Data*, 2003, **48**, 1202–1207.